1

Biomolecular Sensing for Cancer Diagnostics Using Carbon Nanotubes

Jun Li and M. Meyyappan
NASA Ames Research Center, Center for Nanotechnology, Moffett Field, CA 94035

1.1. INTRODUCTION

The field of biomolecule sensing in the medical field is broad and rapidly evolving. The devices range in size from microns to centimeters across the sensing surface and rely on electronic, optical or other form of signals. If the sensing technology utilizes toxic reagents, then the use is limited to only *in vitro* application. In this chapter, biomolecule sensing using carbon nanotubes (CNTs) is discussed with specific application to cancer diagnostics.

Beyond the expected size advantages of the CNT-based sensors, there are other benefits as well. Conventional cytogenetic analysis and fluorescence *in situ* hybridization (FISH) take about three weeks for completion of the analysis. Molecular diagnostic arrays by PCR techniques take less time, still about a week. The sensitivity (i.e. ratio of the number of positive cells detected to all cells) of FISH is 5–10% and conventional cytogenetics is about 5%. Most cytogenetics, FISH and molecular diagnostic testing procedures involve bone marrow aspiration that causes pain. A biosensor that utilizes a nanoelectrode (such as CNT based electrode), in principle, can overcome many of these limitations. The CNT-based cancer diagnostics sensor discussed here can provide instantaneous results, facilitating rapid turn around time and chemotherapy dosing regimens. The detection ability can be 1 positive cell in 1000–10000 cells. Current testing is targetted at *in vitro* application and may be extended for *in vivo* diagnostics in the future, eliminating bone marrow aspiration.

The CNT based biosensor consists of a nanoelectrode array fabricated using conventional microfabrication techniques. In this array, each nanotube electrode is functionalized

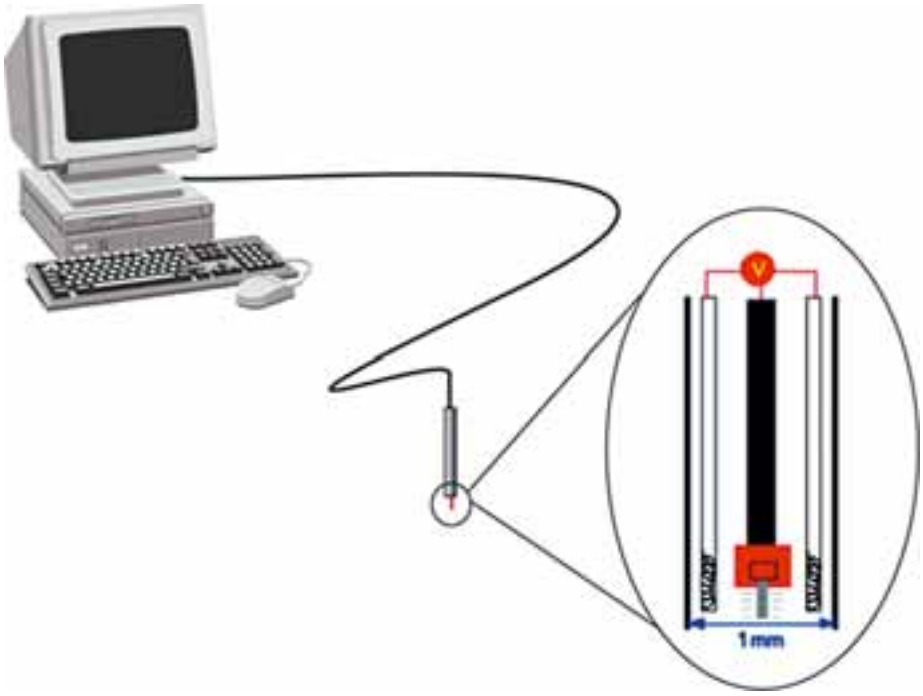

FIGURE 1.1. Schematic of a prototype catheter for cancer diagnostics.

with a probe molecule. The probe-target interaction is captured through the measurement of electrochemical signals amplified by the use of metal-ion mediators.

A proposed design for a biosensor catheter for cancer diagnostics is shown in Fig. 1.1 and the expected operating principle is as follows. The working end of the catheter consists of the carbon nanotube electrode functionalized with the probe molecules. The catheter is inserted into a soft tissue area suspicious for cancer and a pair of external electrodes (shown by the dark outline of the catheter), by applying a current to them, heats and lyzes the cells. The DNA from cancerous cell diffuses towards the stationary probe molecules and the hybridization is detected as an electrochemical signal.

In the sections below, discussion of carbon nanotubes and their interesting properties, nanoelectrode fabrication, testing and characterization are discussed, as a progress report in the fabrication of the biosensor Catheter.

1.2. CARBON NANOTUBES

For a detailed discussion on the properties, growth and applications of carbon nanotubes, the reader is referred to [1]; here, only a brief overview is provided. A carbon nanotube is an elongated fullerene molecule with diameter as small as 7 Å. Configurationally, a nanotube is equivalent to a sheet of graphite rolled into a tube. The resulting single-walled carbon nanotube (SWCNT) is denoted by its chiral vector (n, m) where n and m are indices in the graphene sheet lattice vector. When (n-m)/3 is an integer, the resulting

tube is metallic; otherwise, it is a semiconductor. Besides this intriguing electrical property, the SWCNT is mechanically very strong. It exhibits an Young's modulus of over 1 TPa. The strength/weight ratio of SWCNT is about 600 times higher than that of steel. The maximum strain is about 10% which is higher than that of any other material. Thermal conductivity along the axis of the tube is very high, exhibiting a value upto 3000 W/mK. The conductivity and current carrying capacity are much higher than that of metals such as copper.

A MWCNT is a set of concentric cylinders with a central core where the wall separation is close to 0.34nm. Some of the properties discussed above drop off from the values of SWCNT, nevertheless high enough to create excitement in the research community for a variety of applications. Both SWCNTs and MWCNTs were first produced by an arc discharge synthesis [2]. But for most applications involving devices, electrodes, sensors etc, chemical vapor deposition (CVD) has emerged as a powerful alternative [3]. CVD allows *in situ* growth on a patterned substrate with possibility of subsequent processing steps in an assembly-like fashion. Variations of CVD with the use of a glow discharge have also emerged and this popular plasma enhanced CVD or PECVD has been used to grow individual, free-standing, vertically- aligned multiwalled tubes [3]. For the most part, the PECVD-grown nanostructures tend to have the hollow core periodically interrupted by a bamboo-like closure. The resulting structure is somewhat inferior when it comes to electron transport compared to an ideal MWCNT as electrons have to hop across these closures. In the literature, these structures are called multiwalled carbon nanofibers (MWCNFs) or simply carbon nanofibers (CNFs). In the remainder of this chapter, for generality, they are referred to as MWCNTs.

While the various forms of CNTs are chemically inert, their ends and sidewalls are amenable for attaching a variety of chemical groups. All these interesting structural, mechanical, electrical, thermal and other properties have led to an incredible array of application development. SWCNT based diodes and transistors have been constructed showing interesting electronic properties for memory and logic applications. Interconnects for wiring electronic circuits using nanotubes have been investigated. Potential for near term application with a mass market appeal exists with CNT based field emitters for flat panel TV displays. On the structural side there is active research in developing high strength, low weight polymer matrix, metal matrix and ceramic matrix composites with applications in automotive, aerospace, and construction industries. The ability to functionalize CNTs mentioned above opens up the possibilities to developing chemical sensors and biosensors. The biosensors can serve the needs in biomedical, homeland security, and astrobiology applications.

1.3. CARBON NANOTUBE ELECTRODES

1.3.1. Characteristics of a Good Electrode

Electrodes of all sizes using metals, various forms of carbon and other materials have been around for a variety of applications. Typical expectations of a good electrode and related issues are as follows:

- Appropriate level of conductivity for the chosen application
- The right size to meet the needs
- Ease of fabrication

- Reliability: lifetime, wear characteristics
- Compatibility with the environment
- Signal processing issues: integrity, signal-to-noise, cross-talk in an ensemble
- Approach: electrical vs. electrochemical
- Integration into a functional system

1.3.2. Why Use Nanoelectrode?

The sensitivity of an electrode is mainly determined by its ***signal to noise ratio***. The noise is the background current mainly due to the capacitive charging/discharging current at the electrode/electrolyte interface and thus proportional to the surface area (A) of the electrode as given by:

$$\mathrm{i_n} \propto \mathrm{C_d}^0 \mathrm{A} \tag{1.1}$$

where $\mathrm{C_d}^0$ is the specific capacitance at the interface. In voltammetry measurements, the magnitude of the peak current of the redox signal is the sum of two terms: a linear diffusion as described in the Cottrell equation, and a nonlinear radial diffusion [4]:

$$\mathrm{i_{1,peak}} = nFAC_0 * \sqrt{\frac{D_0}{\pi t}} + nFAC_0 * \left(\frac{D_0}{r}\right) \tag{1.2}$$

where $\mathrm{i}_{l,peak}$ is the diffusion-limited electrical current, n is the number of electrons involved in the reaction with one electroactive species, F is the Faraday constant, C_o is the electroactive species concentration, D_o is the diffusion coefficient, t is time, and r is the radius of the electrode. Both terms are proportional to the concentration of the species present in the solution. The first term is proportional to the electrode surface area and decays to zero over time, whereas the second term is proportional to the inverse of the electrode radius and represents a steady state current due to a constant flux of material to the surface. The ratio of the second term to the first becomes larger as the radius is decreased. The second term dominates the measured peak current, $i_{l,peak}$ if the electrode size is less than 25 μm, which is commonly referred as ultramicroelectrode (UME) [5]. In this regime, the magnitude of the current decreases, but the signal-to-noise ratio is improved as the electrode size decreases, according to:

$$\mathrm{i_{l,peak}}/\mathrm{i_n} \propto nFC_oD_o/r \tag{1.3}$$

Clearly, ***the signal to noise will be improved by 1000 times*** if the electrode size is reduced from 20 μm to 20 nm.

The response time of an electrode is also a function of the electrode dimension. The cell time constant can be described as

$$\tau = \mathrm{R_u C_d} = \mathrm{r C_d}^0/4\kappa \tag{1.4}$$

where κ is the conductivity of the electrolyte. The electrode can ***respond 1000 times faster*** when the size is reduced from microns to nanometers so that fast electrochemical techniques can be applied. The electrochemical signal is defined by the total number of electrons that can be transferred between the electroactive species and the electrode. For high sensitivity

analytical applications, this number is always limited. By employing fast electrochemical techniques, the same amount of electrons can be transferred to the measuring circuit in a much shorter time. As a result, the current, i.e. the real physical quantity being measured, will be much larger and can be differentiated much easier from the background noise.

From the above discussion, it is clear that the performance of an electrode with respect to temporal and spatial resolution scales inversely with the electrode radius. Therefore, the sensitivity can be dramatically improved by reducing the size of the electrodes to nanoscale. Indeed, a single redox molecule was detected using a Pt-Ir electrode with a diameter of 15 nm [6]. With the diameter approaching the size of the target molecules, nanoelectrodes can also interrogate biomolecules much more efficiently than conventional electrodes. There have been strong efforts in developing nanoelectrode based chemical and biosensors since 1980s. However, a reliable method to fabricate nanoelectrodes was lacking until the recent reports of CNT nanoelectrode fabrication using microfabrication approaches discussed below.

1.3.3. Why Use Carbon Nanotubes?

The outside diameter of a MWCNT varies from a few nanometers to about 200 nanometers and the length varies from a few microns to hundreds of microns. The physical dimension of MWCNTs is ideal for fabricating nanoelectrodes, with the dimension approaching the size of biomolecules. MWCNTs normally show highly conductive metallic properties. The open end is an ideal electrode similar to graphite edge plane, while the sidewall is very inert similar to graphite basal plane. The difference in electron transfer rate (ETR) between the open end and the sidewall differs by 5 to 6 orders of magnitude [7]. This makes MWCNT an ideal nanoelectrode which can pick up the signal at the tip and transfer it to the measuring unit connected at the other end with minimum interference by the surrounding environment.

From an electrochemical point of view, CNTs possess great properties similar to commonly used carbon electrodes (particularly for biosensors) such as fast electron transfer rate, wide potential window, flexible surface chemistry, and good biocompatibility. Only a few materials can provide such properties, necessary for maximizing the signal from detecting species while minimizing the noise from other species in the solution. For example, a metal electrode of Pt or Au will electrolyze water before reaching the electropotential needed for the detection of many biomolecules. This causes a large background current that masks out the real signal. Such problems can be avoided by using carbon as the electrode material. The dangling carbon bonds at the open end of a CNT can form various oxides similar to the edge of a graphite sheet, as shown in Fig. 1.2. With electrochemical etching or acid treatment, most dangling bonds can be further converted into -COOH for highly selective functionalization of biomolecules through the formation of amide bonds [8]. While it has been known for sometime that a CNT, particularly a MWCNT, is ideal for biosensing, *the major challenge is how to fabricate and integrate it as a nanoelectrode*. This is discussed in the next section.

1.3.4. Fabrication of CNT Nanoelectrodes

In principle, a single MWCNT can be grown on each individually addressed microelectrode indicated in Fig. 1.3 and used as a nanoelectrode. The microelectrode is more precisely referred to as a ***microcontact*** since it only provides an electrical contact with the MWCNTs. However, the use of individual CNTs is not reliable due to the large fluctuation

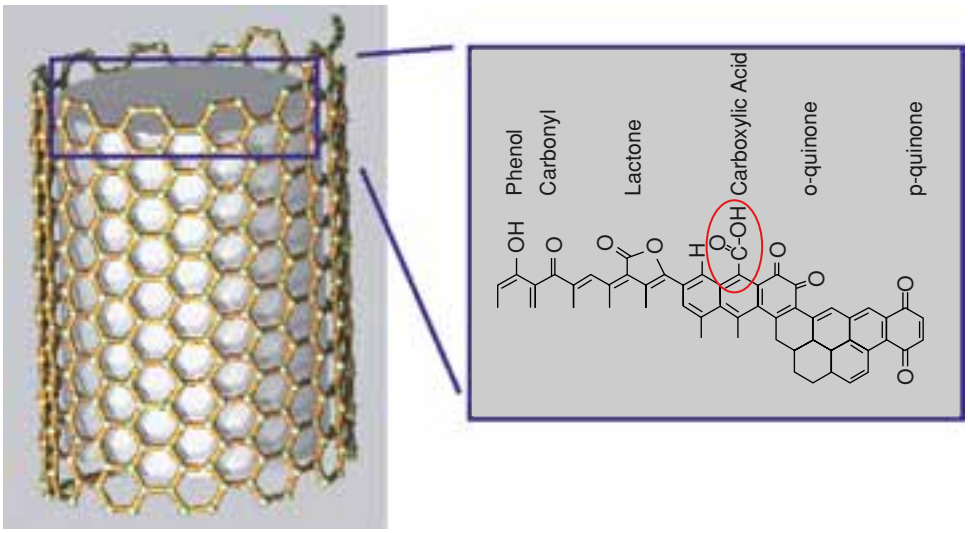

FIGURE 1.2. The functional groups at the open end of a carbon nanotube.

in the detected signal. The signal is also very weak that can be easily masked out by the electronic noises in the environment. These problems can be solved by using an array of nanoelectrodes on each microcontact, as shown in Fig. 1.3. The small circles within each microcontact in Fig. 1.3(a) represent a vertically aligned MWCNT. The side view indicates that such a MWCNT array is embedded in an insulating matrix such as SiO_2 exposing only the very end of MWCNTs to the solution. The other end of the MWCNT is attached to the micron sized metal substrate and wired out to the measuring circuit. For a microcontact with

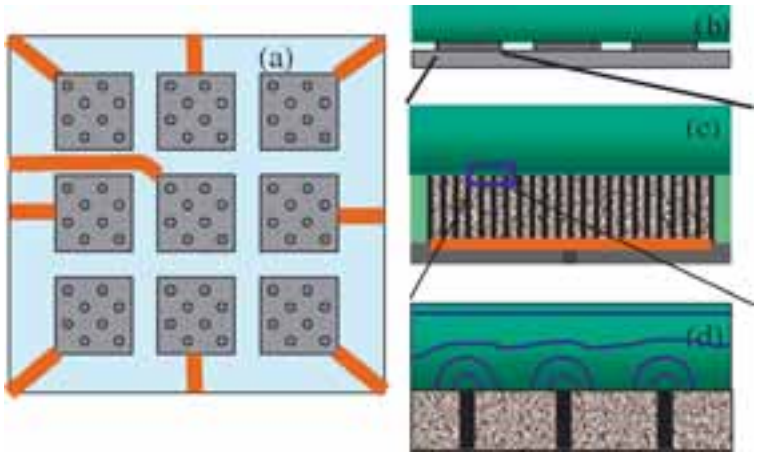

FIGURE 1.3. Schematic of a CNT nanoelectrode chip. (a) top view, (b) cross-sectional view, and (c) enlarged cross-sectional view of MWCNT nanoelectrode array on a single microcontact spot. (d) illustration of the diffusion layer around each MWCNT nanoelectrode.

a size of 20 × 20 μm^2, hundreds to thousands of MWCNT can be grown, which provide enough statistics to improve the reliability. Such array-in-array can provide both extremely high sensitivity and reliability in a multiplexed system.

In a nanoelectrode array (see Fig. 1.3(c) and 3(d)), each electrode can generate a hemispherical layer with a concentration gradient (referred as the diffusion layer) if it is applied with an electropotential that can generate the electrochemical reaction of the species in the solution. The diffusion layer thickness is given by 6 $(Dt)^{0.5}$. The diffusion layers of the neighboring nanoelectrodes would overlap with each other in a high density array. High-density nanoelectrode arrays have been fabricated by filling metals in the channels of filtration membranes and even these high density nanoelectrodes have shown orders of magnitude lower detection limits compared to conventional macroelectrodes (1.6 nM vs 1.6 μM) [9]. Reducing the density can ensure that neighboring electrodes do not interfere with each other and each would truly behave as an individual nanoelectrode, which should give much higher sensitivity. However, this would require a spacing of over 1.5 μm for nanoelectrodes with the diameter of 100 nm, which was not possible with the fabrication method in previous studies. In contrast, a low density nanoelectrode array can be fabricated using MWCNTs with an average tube-tube spacing over 2.5 μm.

For CNT electrode sensors, the signal should ideally occur at the tip of the MWCNT and the transport is through the axial direction to underlying metal microcontacts. The underlying metal and the sidewall of MWCNTs need to be insulated with dielectric materials such as SiO_2. This provides the necessary electrical isolation of individual nanoelectrodes in addition to an overall mechanical robustness. A bottom-up approach to fabricate this electrode array is described below [10, 11]. The sequence of processing steps is shown in Fig. 1.4. A given electrode can have many vertically aligned MWCNTs at pre-specified

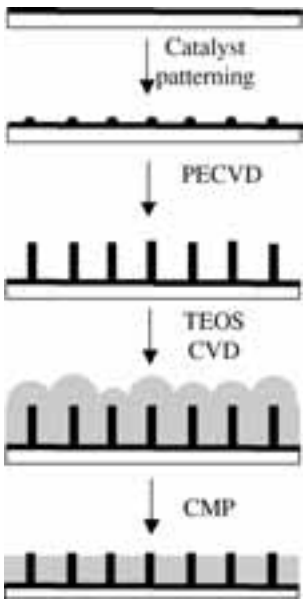

FIGURE 1.4. Schematic of the fabrication of CNT nanoelectrode array for biosensing.

locations to form an array electrode. Therefore, the first two steps would be the growth of the vertical MWCNTs and the insulation of individual MWCNTs with dielectric materials. A chemical mechanical polishing (CMP) step will be then applied to produce a smooth top surface and expose only the very ends of the MWCNTs. A dc plasma reactor with a hot filament (dc-HFCVD) has been used to obtain individual, freestanding, vertically aligned MWCNTs [12]. The feedstock for CNT growth is acetylene diluted in ammonia. Catalyst patterning is done using ion beam sputtering to deposit a thin layer of Ni on silicon substrates. Addition of an underlayer of Cr or similar metal first allows tuning the final conductivity as well as providing a barrier layer to prevent diffusion of Ni catalyst into the substrates.

The variables in the growth process include plasma power, choice of feedstock, total flow rate, ratio of active gas to diluents, growth temperature, additional bias on the substrate, and growth time. In addition, the choice for catalyst metal and its thickness, choice of underlayers and its thickness, and approach to deposit the catalyst also dictate the outcome [3]. The expected output parameters are CNT density, CNT diameter, CNT height, growth on pre-specified locations if desired, maintaining pre-specified distance between nanotubes through patterning if desired, material characteristics and conductivity, and good contact with the substrate.

Once the MWCNTs are grown on the substrate, a dielectric material can be used to isolate them from one another. The integrated circuit (IC) community has used SiO_2, some nitrides and spin-on-glass for similar purposes. Of these, SiO_2 meets the necessary isolation requirements and can be readily deposited using thermal CVD. Tetraethoxysilane (TEOS) is routinely used as a source gas in thermal CVD of SiO_2 at around 700–800° C and 100–500 mTorr. This process known as 'gap-filling' is common in IC manufacturing. The desirable outcome is to fill the gap completely without voids and provide the needed isolation characteristics. This depends on the inter-distance of the nanotubes in the array and the conformality of the dielectrics. Control on this can be exercised through growth temperature, reactor pressure, TEOS flow rate, and growth time. As seen in the process schematic (Fig. 1.4), the oxide dielectric fills the gaps, wraps around individual nanotubes (i.e. bury the nanotubes), and covers the substrate surface. A third step involving CMP is needed to remove the excess SiO_2 and expose the nanotubes. This should provide a flat surface with only the very end of MWCNTs exposed as inlaid nanodisk electrodes in the insulating SiO_2 matrix.

The fabricated electrodes can be characterized using a number of techniques. Scanning electron microscopy (SEM) provides top and perspective images of the embedded CNT array electrode as shown in Fig. 1.5. An atomic force microscope (AFM) with current sensing module (CS-AFM) can be used to measure the current-voltage (I-V) characteristics of individual nanotubes. As will be seen in the next sections, this characterication shows that MWCNTs are highly conductive metallic wires with good electrical contact with the underlying metal film. This ensures that the exposed MWCNT can be used as a good nanoelectrode.

1.4. PRELIMINARY RESULTS

1.4.1. Electronic Nano-Chip Development

As a first step for developing a multiplex electronic chip, a 3×3 array was successfully designed and fabricated using the procedure described above [8, 12]. Figures. 1.6(a) and (b)

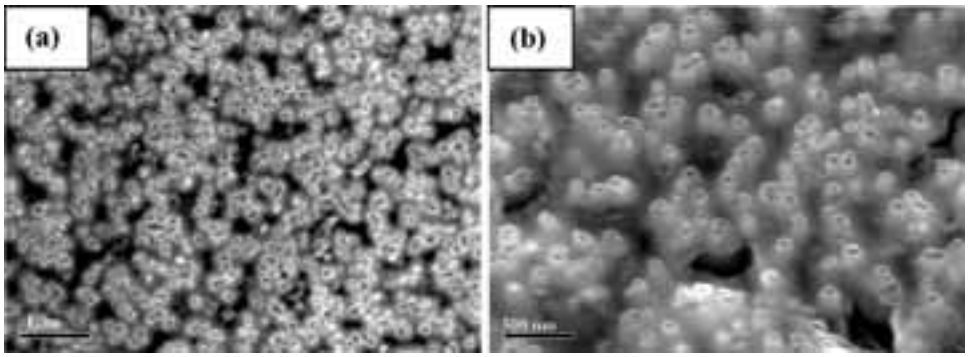

FIGURE 1.5. Scanning electron microscopy (SEM) images of a planarized CNT nanoelectrode array embedded in SiO_2 matrix. (a) top view and (b) 45° perspective view.

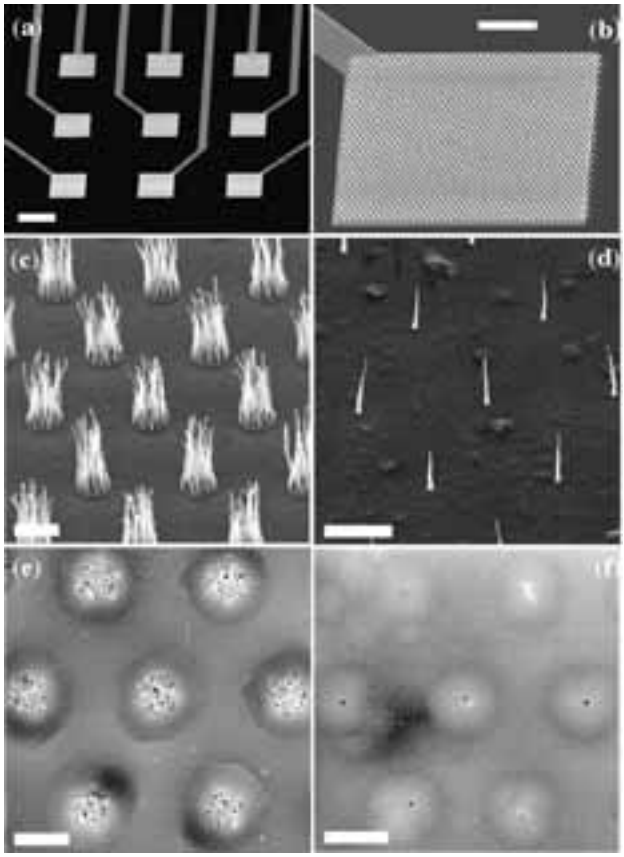

FIGURE 1.6. SEM images if (a) a 3 × 3 electrode array, (b) array of MWCNT bundles on one of the electrode pads, (c) and (d) array of MWCNTs on UV-lithography and e-beam patterned Ni spots respectively, (e) and (f) the surface of polished MWCNT array electrodes grown on 2 μm and 200 nm spots respectively. (a)–(d) are 45° perspective views and (e)–(f) are top views. The scale bars are 200, 50, 2, 5, 2, and 2 μm, respectively.

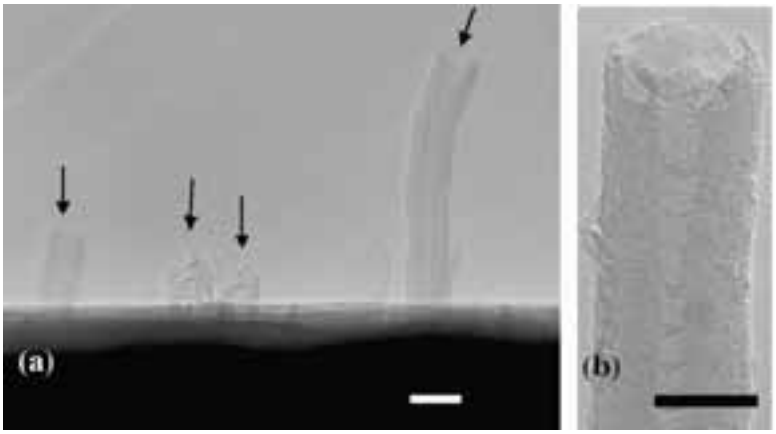

FIGURE 1.7. TEM images of MWCNT arrays after chemical mechanical polishing showing the graphite edge-plane like open ends. The scale bars are 50 and 20 nm.

show SEM images of a 3 × 3 array of individually addressed electrodes on a Si(100) wafer covered with 500 nm thermal oxide. The electrodes and contact lines are 200 nm thick Cr patterned with UV-lithography. Each electrode can be varied from 2 × 2 to 200 × 200 μm^2, consisting of a vertically aligned MWCNT array grown by PECVD from 10–20 nm thick Ni catalyst films. Figs. 1.6(c) and (d) show MWCNT arrays grown on 2μm and 200 nm diameter Ni spots defined by UV and e-beam lithography respectively. The spacing and spot size can be precisely controlled. The diameter of the MWCNTs is uniform over the whole chip and can be controlled between 30 to 100 nm by varying PECVD conditions. The number of CNTs at each spot can be varied as well by changing the thickness of the Ni film. Single nanotubes can be grown at each catalyst spots if their size is reduced below 100 nm. An SiO_2 gap-fill process described earlier has been used to encapsulate each nanotube and the substrate surface with a conformal SiO_2 film, resulting in a mechanically stable and well-insulated matrix, followed by CMP to expose the very end of the CNTs. Figs. 1.6(e) and (f) show the embedded CNT array electrodes with different patterns after polishing. Clearly, CNTs retain their integrity and are separated from each other. As shown in Fig. 1.7, the as-polished samples show CNTs protruding above the SiO_2 matrix by about 30–50 nm due to their high mechanical resilience. An electrochemical (EC) etching step is employed to shorten the exposed nanotubes and level them to the same plane as the SiO_2 matrix, exposing minimum CNT surface area. The PECVD grown MWCNTs have a bamboo-like structure with a series of closed shells along the tube, which seal off most of the hollow channel, leaving only the very end accessible by electrolytes (see Fig. 1.7b).

In general, it is too expensive to fabricate reliable nanoelectrode arrays with desired low-density using advanced lithography based on e-beam, EUV, and focused ion beam. However, since MWCNTs in the as-grown array typically have uniform diameter but varying heights, different densities can be easily obtained by stopping CMP at the proper stage. Figure. 1.8(a) shows a SEM image of a MWCNT array right after encapsulating in SiO_2 grains. During CMP, more and more MWCNTs are exposed as shown in Fig. 1.8(b)–(d), which can be easily monitored by measuring the electrical resistance (R) between two points at the surface. A

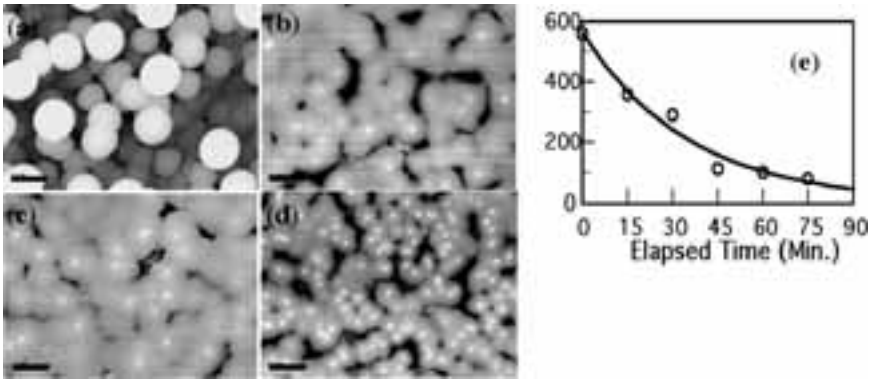

FIGURE 1.8. SEM images of (a) an as-encapsulated MWCNT array in SiO_2, and (b)–(d) the polished surface showing the number of exposed MWCNT increasing with the progress of CMP. All scale bars are 1 μm (e) The calibration curve used for controlling the density of exposed MWCNTs.

calibration curve in Fig. 1.8(e) shows the value of R vs. the elapsed time during the final stage of CMP. The resistance R drops exponentially with time and saturates at about 50 to 80 Ohm, where almost all MWCNTs are exposed. If R is controlled over 400 Ohm, a low-density MWCNT nanoelectrode array with an average tube-tube distance over 2.5 μm is readily fabricated. This method makes it possible to mass-produce nano-chips at minimum cost so that it can be used as a disposable cartridge for cancer diagnosis.

1.4.2. Electrochemical Properties of CNT Nanoelectrode Arrays

The MWCNT nanoelectrode array fabricated above has been carefully characterized with electrochemical (EC) measurements. The measurements are carried out in a three-electrode configuration by sealing the CNT array chip in a TEFLON cell using a 3 mm i.d. o-ring. A Pt coil and a saturated calomel electrode (SCE) are used as the counter and reference electrodes, respectively. Two MWCNT nanoelectrode arrays with average spacing of ∼280 nm and 1.5 μm are compared side-by-side in measuring $K_4[Fe(CN)_6]$ in bulk solution and $Fc(CH_2)_2NH_2$ covalently attached to the exposed end of CNTs. As shown in Fig. 1.9, the high-density sample exhibits a typical cyclic voltammetry (CV) curve with a pair of redox peaks centered at the characteristic potential corresponding to $K_4[Fe(CN)_6]$ while the low-density sample gives a sigmoidal shaped CV curve. This confirms that the diffusion layer from an individual nanoelectrode in the high density sample completely overlaps with those of its neighbors, giving the characteristic CV similar to a solid macroelectrode. On the other hand, the majority of MWCNTs in the low-density sample remains as individual nanoelectrodes and are able to reach the characteristic steady state above certain potentials. As for surface attached ferrocene (Fc) molecules, the signal is much weaker because the total number of Fc decreases as the CNT density is lowered. A pair of redox waves separated by about 30 mV is observed with the high-density sample indicating a quasireversible behavior of surface binded redox species. The signal is so low for the low-density sample that it is masked out by the background noise. A special EC technique, AC voltammetry can be employed to maximize the signal contributed by each redox species as shown in

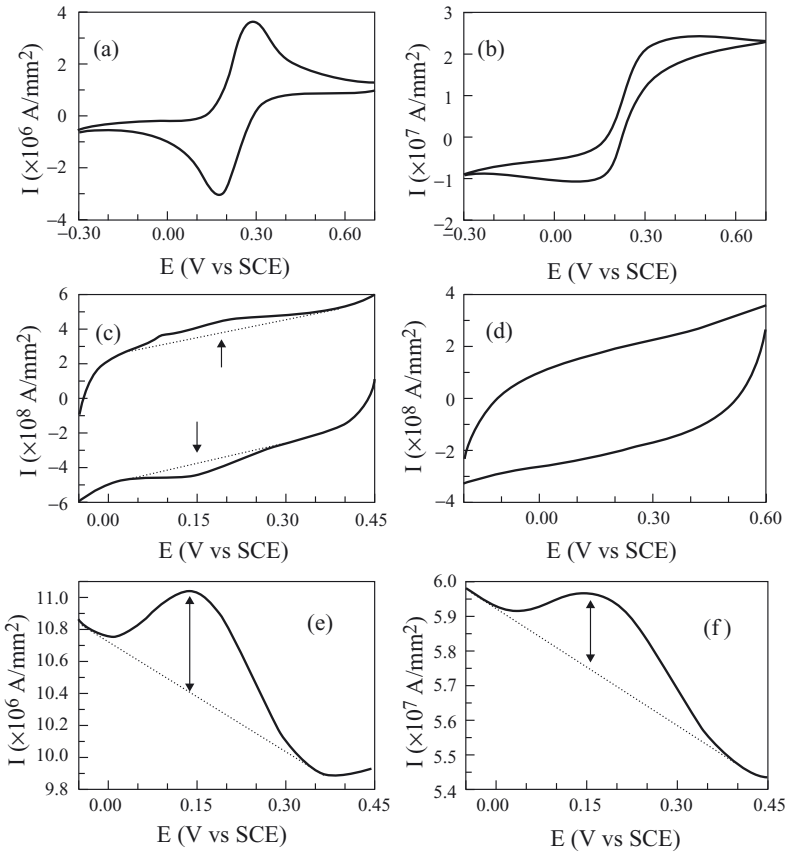

FIGURE 1.9. (a), (b) CV measurements in 1 mM $K_4Fe(CN)_6$ and 1.0 M KCI; (c), (d) CV measurements of Fc derivative functionalized MWCNT array electrodes in 1.0 M KCI solution; and (e), (f) ACV measurements at 50 Hz and an amplitude of 50 mV on the staircase DC ramp from −0.05 to 0.45 V (a), (c), (e) are measured with the high-density CNT array electrode and (b), (d), (f) are measured with the low density one, respectively. All CV measurements are taken with a scan rate of 20 mV/s. The arrows indicate the position of the redox waves of the Fc derivative functionalized on the high-density CNT array elecrode. The dotted lines indicate the baselines of the background current.

Figs. 1.9(e) and (f). Clearly, the signal is much bigger than that obtained using conventional DC voltammetry. Thus AC voltammetry will be the ideal technique for biosensors based on nanoelectrode array.

1.4.3. Functionalization of Oligonucleotide Probes

As mentioned earlier, the oxides at the CNT ends can be converted to carboxylic groups using EC etching. A ferrocene (Fc) derivative, $Fc(CH_2)_2NH_2$, can be selectively functionalized at the tube ends through amide bonds facilitated by the coupling reagents dicyclohexylcarbodiimide (DCC) and N-hydroxysuccinimide (NHS) [13] as illustrated in Fig. 1.10(a). Similar carbodiimide chemistry can be applied to functionalize primary amine

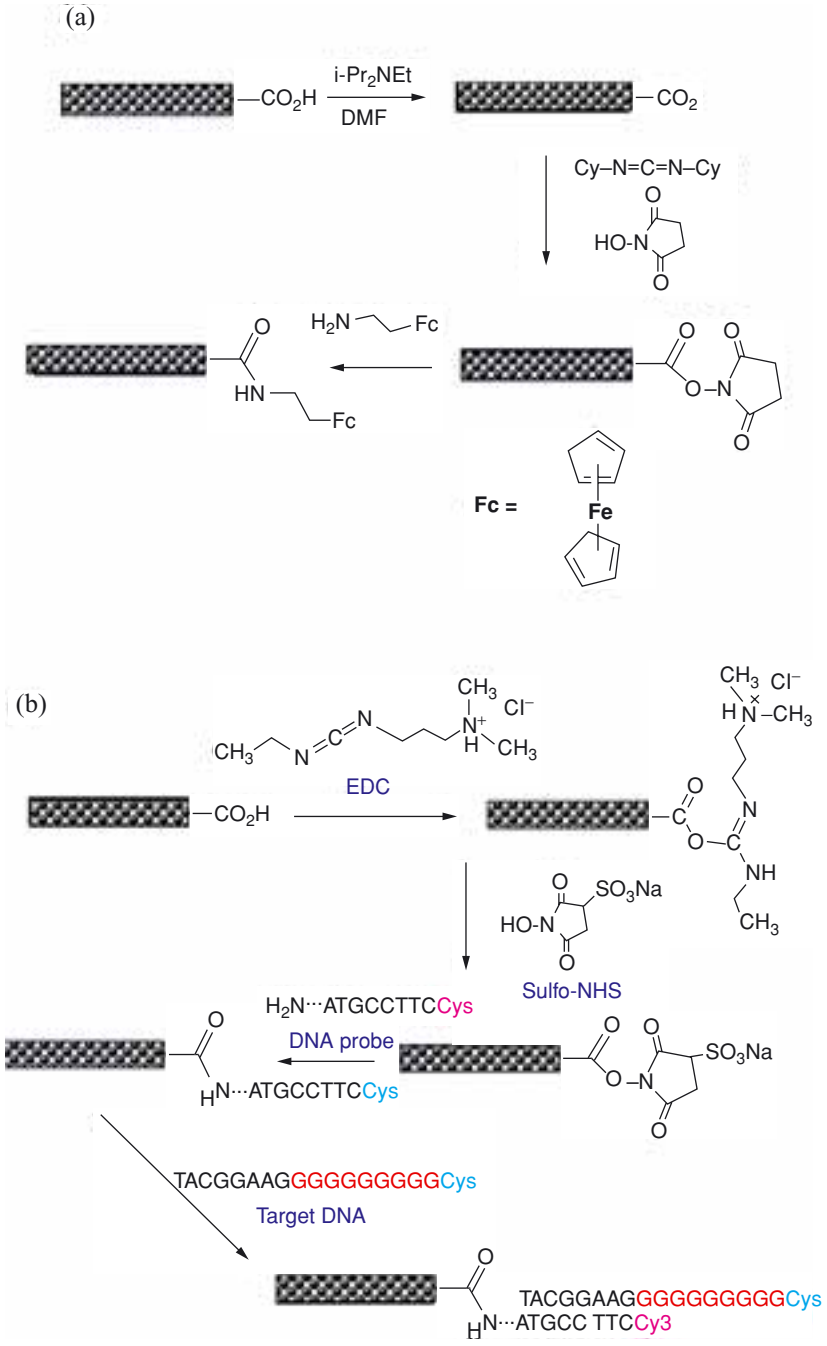

FIGURE 1.10. The schematic of functionalization of (a) ferrocene derivative and (b) oligonucleotide probe to the end of a CNT through the formation of amide bonds.

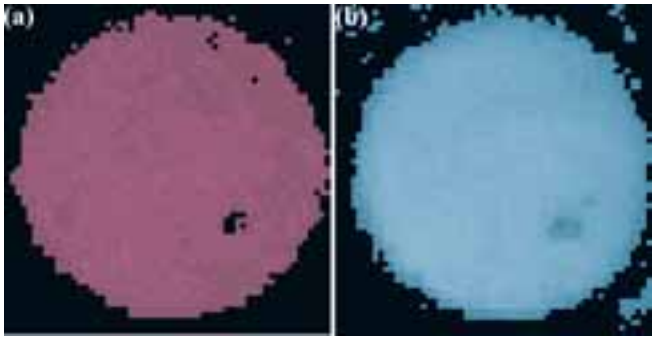

FIGURE 1.11. The fluorescence images of (a) Cy3 (from the probe) and (b) Cy5 (from the target) after the functionalization, hybridization, and washing steps. The probe functionalization was confined within a 3 mm i.d. o-ring.

terminated oligonucleotides using water-soluble coupling reagents 1-ethyl-3(3-dimethyl aminopropyl carbodiimide hydrochloride (EDC) and N-hydroxysulfo-succinimide (sulfo-NHS) as shown in Fig. 1.10(b). A probe [Cy3]5'-CTIIATTTCICAIITCCT-3'[AmC7-Q] and a target [Cy5]5'-AGGACCTGCGAAATCCAGGGGGGGGGGG-3' are used, which are related to the wild type gene of BRCA1 Arg1443stop [14]. Fluorescence images of Cy3 and Cy5 labels are taken with a laser scanner after each step of functionalization, hybridization, and washing to confirm the attachment. Figure 1.11 shows the Cy3 and Cy5 images obtained on a MWCNT chip of 1×1 cm^2 after hybridization and washing. The probe functionalization was confined within a 3 mm inner diameter o-ring but the hybridization was carried out by incubating the whole chip in the target solution. Clearly, the target binds to the surface only through specific hybridization with the probe. Nonspecific binding was removed by washing procedures.

1.4.4. Electrochemical Detection of DNA Hybridization

It has been reported that the guanine bases in DNA can be oxidized at $\sim$1.05 V [15] and this oxidation reaction can be used for DNA detection [16]. An electrochemical detection using an oligonucleotide target has been demonstrated as shown in Fig. 1.10(b). A 10 bp polyG tag is attached to the sequence fully matched with the probe, which serves as the signal moiety. The guanine bases in the probe are replaced with inosine to ensure no guanine contribution from the probe. To further amplify the guanine oxidation signal, a mediator $Ru(bpy)_3{}^{2+}$ is introduced which can transfer electrons from the guanine bases dangling near the electrode surface as schematically illustrated in Fig. 1.12. Combining together the advantages of nanoelectrode array, guanine oxidation, mediator amplification, and AC voltammetry, extremely high sensitivity of EC detection has been achieved. The net AC voltammetry data is presented in Fig. 1.13(a). In scaling down with a MWCNT array on a 20×20 μm^2 microcontact, *less than 10^6 of oligonucleotide targets* attached to this spot could be easily detected. This number is the maximum estimation, while the real number of target DNA detected could be orders of magnitude smaller.

It has also been demonstrated that PCR amplicon could be directly used for EC detection using CNT nanoelectrode arrays. The same BRCA1 gene probe is employed for

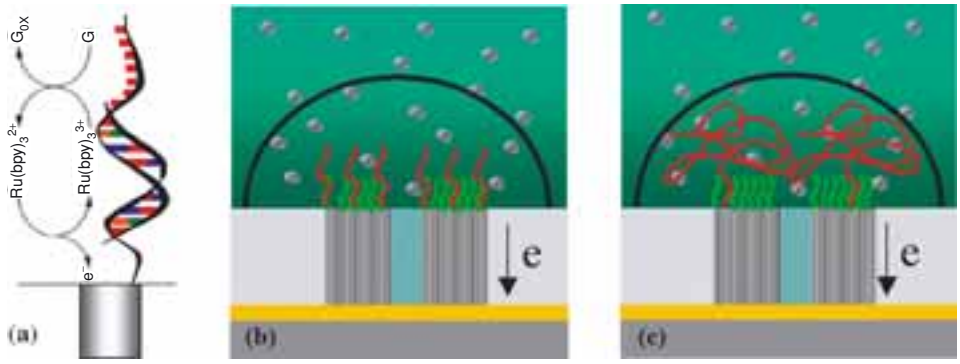

FIGURE 1.12. The schematic of (a) the mechanism of $Ru(bpy)_3^{2+}$ mediator amplified guanine oxidation, (b) the detection of oligonucleotide targets, and (c) PCR amplicon targets.

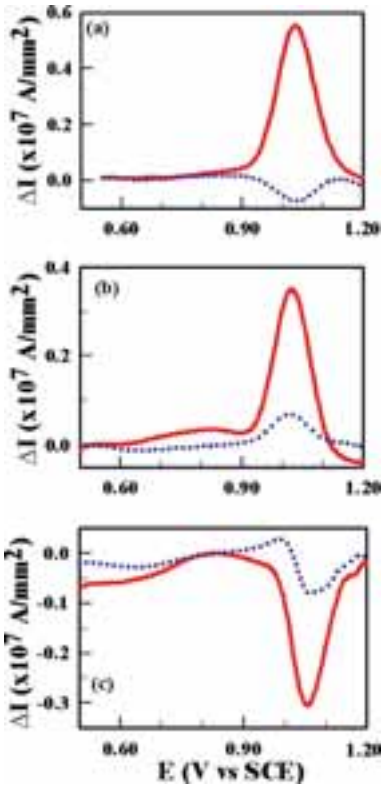

FIGURE 1.13. The net AC voltammetry data and control measurements in 5 mM Ru $(bpy)_3^{2+}$ and 0.20 M NaOAC (pH = 5.2) with an AC sinusoidal wave of 10 Hz and 25 mV amplitude on top of a staircase DC ramp after incubation in (a) specific polyG tagged oligonucleotide target, (b) specific PCR amplicon, and (c) non related PCR amplicon.

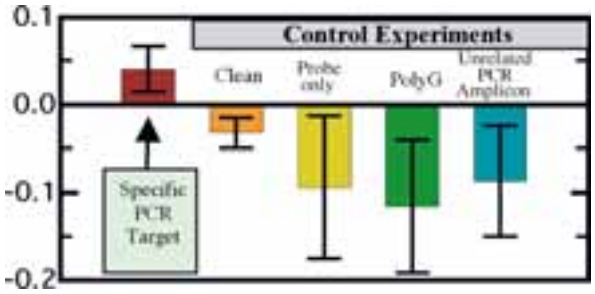

FIGURE 1.14. The summary of the mean value and the standard deviation of the normalized net ACV data $(I_{p1}-I_{p2})/I_{p1}$ from 21 measurements at five different conditions.

this. But the target is changed to ∼300 bp normal allele within BRCA1 gene containing 5'-AGGACCTGCGAAATCCAG-3' which is complementary to the specific oligonucleotide probe. Genomic DNA from a healthy donor is used in PCR amplification. Considering the physical size (radius of gyration of ∼6 nm for 300 bp ssDNA), it is expected that no more than ∼70 targets can hybridized with the probes on each MWCNT of ∼100 nm dia. The nonspecific binding is removed by stringent washing with 2 × SSC/0.1%SDS, 1 × SSC, and 0.1% SSC at 40° C for 15 min., respectively. The major part of the target molecules likely dangles near but may not be necessarily be in direct contact with the electrode surface as shown in Fig. 1.12(c). $Ru(bpy)_3^{2+}$ mediators can efficiently transport electrons from the guanine bases to MWCNT nanoelectrodes to provide an amplified guanine oxidation signal as long as target DNA molecules are within the three-dimensional diffusion layer (typically a hemisphere with a radius of ∼300 nm, i.e. $\sim 6R_{ave}$, where R_{ave} is the average nanoelectrode radius). Since the PCR amplicon is quite long (∼ 300 bp) and statistically contains ∼75 guanine bases, the same level of net EC signal is obtained, as shown in Fig. 1.13(b) compared to the 10 bp polyG tagged oligonucleotide target even though the number of targets is much less. Sensitivity for detecting less than 1000 target molecules can be achieved using a $20 \times 20\,\mu m^2$ microcontact. A sample that has gone through the same incubation condition in nonrelated ∼400 bp PCR amplicon gives negative net EC signal as seen in Fig. 1.13(c). Figure 1.14 summarizes 21 experiments at five conditions. It clearly shows positive EC signal for specific targets and negative EC signal in all four control experiments. Such high reliability required for cancer diagnostics has not been reported by using other nanotechnology based DNA sensors.

1.5. SUMMARY

A carbon nanotube based biosensing approach for cancer diagnostics has been described. The motivation for nanoelectrodes and the role of nanotubes in developing an ultrasensitive platform has been elucidated. A progress report on the development of nanoelectrode, characterization, and electrochemical detection of DNA hybridization has been given. The preliminary results indicate the potential of this approach for cancer diagnostics with demonstrated characteristics of high sensitivity, reliability, and inexpensive microfabrication for cost effectiveness.

ACKNOWLEDGEMENTS

The authors are grateful to Alan Cassell, Hua Chen, and Jessica Koehne for their contributions to the biosensor development described here.

REFERENCES

[1] *Carbon Nanotube: Science and Applications*, M. Meyyappan (Ed.), CRC Press, Boca Raton, FL, 2004.
[2] A.P. Moravsky. E.M. Wexler, and R.O. Loutfy, Chapter 3 in ref. 1.
[3] M. Meyyappan. Chapter 4 in ref. 1.
[4] A.J. Bard and L.R. Faulkner. *Electrochemical Methods: Fundamental and Applications*, 2nd Ed. Wiley, New York, 216–218, 2001.
[5] R.M. Wightman. *Anal. Chem*., 53: 1125A, 1981.
[6] F.-R.F. Fan and A.J. Bard. *Science*, 267: 817, 1995.
[7] L. McCreery. *In Electroanalytical Chemistry*, A.J. Bard (Ed.), Marcel Dekker, Inc., New York, 17: 221–374, 1991.
[8] J. Li, H.T. Ng, A. Cassell, W. Fan, H. Chen, Q. Ye, J. Kohene, J. Han, and M. Meyyappan. *Nano Lett.*, 3: 597, 2003.
[9] V. P. Menon and C.R. Martin. *Anal. Chem*., 67: 1920, 1995.
[10] J. Li, R. Stevens, L. Delzeit, H.T. Ng, A. Cassell, J. Han, and M. Meyyappan. *Appl. Phys. Lett.*, 81 (5): 910, 2002.
[11] J. Li, Q.L. Ye, A.M. Cassell, H.T. Ng, R. Stevens, J. Han, and M. Meyyappan. *Appl. Phys. Lett.*, 82 (15): 2491, 2003.
[12] A.M. Cassell, Q. Ye, B.A. Cruden, J. Li, P.C. Sarrazin, H.T. Ng, J. Han, and M. Meyyappan. *Nanotechnology*, 15: 9, 2004.
[13] J.V. Staros. *Biochemistry*, 21: 3950, 1982.
[14] Y. Miki, J. Swensen, D. Shattuck-Eidens, P.A. Futreal, K. Harshman, S. Tavtigian, Q. Liu, C. Cochran, L.M. Bennett and W. Ding. *Science*, 266: 66, 1994.
[15] M.F. Sistare, R.C. Holmberg, and H.H. Thorp. *J. Phys. Chem. B*, 103: 10718, 1999.
[16] N.D. Popovich and H.H. Thorp. Interface, 11 (4): 30, 2002.

http://www.springer.com/978-0-387-25563-7

BioMEMS and Biomedical Nanotechnology
Volume I: Biological and Biomedical Nanotechnology
Editor-in-chief: Ferrari, M. - Lee, A.; Lee, J. (Eds.)
2006, XX, 520 p., Hardcover
ISBN: 978-0-387-25563-7